

Folding and Intramembraneous BRICHOS Binding of the Prosurfactant Protein C Transmembrane Segment*

Received for publication, December 6, 2014, and in revised form, May 30, 2015. Published, JBC Papers in Press, June 3, 2015, DOI 10.1074/jbc.M114.630343

Alejandra Sáenz^{‡§}, Jenny Presto[¶], Patricia Lara[¶], Laura Akinyi-Oloo[¶], Belén García-Fojeda[§], IngMarie Nilsson[¶], Jan Johansson[¶], and Cristina Casals^{‡§}

From the [‡]Department of Biochemistry and Molecular Biology I, Complutense University of Madrid, 28040 Madrid, Spain, the [§]Centro de Investigación Biomédica en Red de Enfermedades Respiratorias (CIBERES), Instituto de Salud Carlos III, 28029 Madrid, Spain, the [¶]Center for Alzheimer Research, NVS (Neurobiology, Care Sciences, and Society) Department, Karolinska Institutet, S-141 57 Huddinge, Sweden, and the [¶]Department of Biochemistry and Biophysics, Center for Biomembrane Research, Stockholm University, S-10691 Stockholm, Sweden

Background: Amyloidogenic human lung surfactant protein C (SP-C) is a transmembrane peptide generated from pro-SP-C, containing a luminal BRICHOS domain.

Results: BRICHOS inserts partly in ER membranes, binds unfolded SP-C, and prevents misfolding.

Conclusion: Disease-associated pro-SP-C mutations result in loss of membrane insertion and binding to SP-C.

Significance: Co-translational folding of transmembrane pro-SP-C is inefficient and membrane insertion of BRICHOS promotes correct folding.

Surfactant protein C (SP-C) is a novel amyloid protein found in the lung tissue of patients suffering from interstitial lung disease (ILD) due to mutations in the gene of the precursor protein pro-SP-C. SP-C is a small α -helical hydrophobic protein with an unusually high content of valine residues. SP-C is prone to convert into β -sheet aggregates, forming amyloid fibrils. Nature's way of solving this folding problem is to include a BRICHOS domain in pro-SP-C, which functions as a chaperone for SP-C during biosynthesis. Mutations in the pro-SP-C BRICHOS domain or linker region lead to amyloid formation of the SP-C protein and ILD. In this study, we used an *in vitro* transcription/translation system to study translocon-mediated folding of the WT pro-SP-C poly-Val and a designed poly-Leu transmembrane (TM) segment in the endoplasmic reticulum (ER) membrane. Furthermore, to understand how the pro-SP-C BRICHOS domain present in the ER lumen can interact with the TM segment of pro-SP-C, we studied the membrane insertion properties of the recombinant form of the pro-SP-C BRICHOS domain and two ILD-associated mutants. The results show that the co-translational folding of the WT pro-SP-C TM segment is inefficient, that the BRICHOS domain inserts into superficial parts of fluid membranes, and that BRICHOS membrane insertion is promoted by poly-Val peptides present in the membrane.

In contrast, one BRICHOS and one non-BRICHOS ILD-associated mutant could not insert into membranes. These findings support a chaperone function of the BRICHOS domain, possibly together with the linker region, during pro-SP-C biosynthesis in the ER.

Surfactant protein C (SP-C)⁴ is an extremely hydrophobic TM peptide that consists of 35 amino acid residues, which are cleaved out from its 197-amino acid precursor, pro-SP-C. SP-C together with phospholipids lowers alveolar surface tension and prevents the lung from collapsing at the end of expiration (1, 2). Pro-SP-C is synthesized as a type II membrane protein, with its N-terminal segment facing the cytosol and the single TM segment inserted into the ER membrane in a co-translational manner (3).

Most eukaryotic membrane proteins insert and fold in the ER membrane (4). In mammalian cells, the insertion process is mediated by a proteinaceous channel, the translocon Sec61, composed of Sec61 α , β , and γ (5–7). Both the hydrophobicity of the TM segments and the charged residues flanking the TM segments play important roles in this process. N-Linked glycosylation is one of the most common types of eukaryotic protein modifications. The attachment of carbohydrates to asparagine in secretory and membrane proteins takes place during co-translational translocation across the ER membrane. The transfer of high mannose oligosaccharides from a dolichol carrier to Asn-X-Thr/Ser acceptor sites is catalyzed by the oligo-

* This work was supported by Spanish Ministry of Economy and Competitiveness Grant SAF2012-32728 and Institute of Health Carlos III (ISCIII) (Spanish Research Center of Respiratory Diseases) Grant CIBERES CB06/06/0002, the Swedish Research Council, Henrik Granholms Stiftelse Grant SU 33-1013-09 (to I. M. N.), Swedish Cancer Society Grant 13624 (to I. M. N.), Swedish Foundation for International Cooperation in Research and Higher Education (STINT) Grants 210/083(12) and KU 2003–4674 (to I. M. N.), Swedish Foundation for Strategic Research Grant A305:200 (to I. M. N.), The Swedish Alzheimer foundation, The Åke Wibergs foundation, The Magn Bergvalls foundation, Foundation of Gamla tjänarinnor, and The Loo and Hans Ostermans foundation for geriatric research. The authors declare that they have no conflicts of interest with the contents of this article.

¹ Both authors contributed equally to this article.

² To whom correspondence may be addressed. E-mail: janne.johansson@ki.se.

³ To whom correspondence may be addressed. Tel.: 34-913944261; Fax: 34-913944672; E-mail: ccasals@ucm.es.

⁴ The abbreviations used are: SP-C, surfactant protein C; TM, transmembrane; ER, endoplasmic reticulum; OST, oligosaccharyltransferase; ILD, interstitial lung disease; DPPC, 1,2-dipalmitoyl-phosphatidylcholine; POPC, 1-palmitoyl-2-oleoyl-phosphatidylcholine; POPG, 1-palmitoyl-2-oleoyl-phosphatidylglycerol; DPH, 1,6-diphenyl-1,3,5-hexatriene; TEMPO, 2,2,6,6-tetramethyl-1-piperidinyloxy; DM, dodecyl- β -D-maltoside; CRM, canine rough microsomes; Endo H, endoglycosidase H; MLV, multilamellar vesicles; LUV, large unilamellar vesicle; DSC, differential scanning calorimetry; MIP, maximum insertion pressure; mN, millinewton.

saccharyltransferase (OST) (8). The OST catalytic site is located on the luminal side of the ER membrane, and the enzyme is located near the translocon, the site of protein translocation and integration in the ER membrane (8).

The C-terminal part of pro-SP-C is localized in the ER lumen and harbors a BRICHOS domain and an ~30-residue linker region that separates the BRICHOS domain from the ER membrane. The BRICHOS domain consists of ~100 amino acid residues and was initially identified in Bri2, chondromodulin and pro-SP-C, but later found to be present in more than 1000 different proteins, divided into families. The overall amino acid sequence conservation of the BRICHOS domain is low, but it shows a well conserved secondary structure pattern (9, 10).

Amyloid-forming proteins give rise to around 30 amyloid diseases, among them Alzheimer disease, prion diseases, and type II diabetes mellitus. Recently SP-C was added to the list of amyloid-forming proteins (11). The TM α -helix of SP-C is discordant, *i.e.* it is predicted to form β -sheets, because it mainly consists of valine residues, which are strongly overrepresented in β -sheets. SP-C can convert into β -strand conformation and form amyloid-like fibrils (12–15). It has been shown that patients with interstitial lung disease (ILD) due to mutations in the pro-SP-C gene have amyloid deposits of SP-C in the lung parenchyma (16). There are about 50 such mutations, and the majority are located in the linker region (such as I73T mutation) and the BRICHOS domain (such as L188Q mutation). It was suggested that mutations that abrogate a chaperone-like function of the BRICHOS domain in pro-SP-C lead to misfolding of the SP-C TM segment (16).

The first step in the folding of any TM protein, such as pro-SP-C, begins with the coordinated action of the ribosome-translocon complex. It has previously been shown that a model poly-Val segment is less efficient in forming an α -helix in the ribosome and ER translocon than a poly-Leu segment, which folds into an α -helix already in the ribosome (17). Poly-Leu substitution for poly-Val in a synthetic analog of SP-C resulted in a dramatic increase in spontaneous formation of a stable α helix (14, 18). In addition, expression in a cell line of pro-SP-C with a poly-Leu TM segment instead of the native poly-Val counterpart results in strong reduction of aggregation even in the presence of a non-functional BRICHOS domain carrying an ILD associated mutation (19). The folding of the pro-SP-C TM segments is thus not only of interest in relationship to ILD associated with BRICHOS mutations and amyloid, but also in relationship to general determinants for folding of TM segments.

We have previously proposed that folding of the pro-SP-C TM segment needs to be assisted by a BRICHOS domain, and that this involves capturing the unfolded TM segment in the ER membrane. In this model, binding of the BRICHOS domain to the unstructured poly-Val TM segment inhibits misfolding into a β -sheet, and promotes folding into an α -helix. Helix formation leads to release from the BRICHOS domain, and eventually the correctly folded helical TM region is inserted into the ER membrane (16). Recent results suggest that the BRICHOS domain recognizes motif(s) common to amyloid formation of different peptides, thereby inhibiting formation of amyloid fibrils (20). Moreover, pro-SP-C BRICHOS has also proved

to be very effective as a molecular chaperone against the Alzheimer disease-associated peptide A β , both *in vitro* (20–22) and *in vivo* (23). Recently, pro-SP-C BRICHOS was found to specifically block the secondary nucleation step in A β fibril formation, with important implications for its ability to block amyloid toxicity (24).

The amyloid deposits found in patients with ILD consist of SP-C peptide, but it has not been shown where or at what stage of SP-C biosynthesis these deposits are formed. Misfolding and aggregation may start already in the translocon and/or the ER membrane, and recent results support that the latter is the case for some, but not all, pro-SP-C mutations associated with ILD (25). Moreover, how the water-soluble BRICHOS domain manages to interact with the hydrophobic pro-SP-C TM segment in the membrane is not understood. We have previously reported that pro-SP-C BRICHOS binds to phospholipids and that the binding induces increased disorder in the BRICHOS structure (26). Here we have used translocon-mediated *in vitro* translation and a minimal glycosylation distance assay to study folding of the pro-SP-C TM segment in the ER membrane, by measuring how efficiently native poly-Val and designed poly-Leu segments fold into compact, helical conformation. Moreover, we have also studied if the pro-SP-C BRICHOS domain inserts into the ER membrane. To this end we investigated the recombinant human WT pro-SP-C BRICHOS domain and two ILD-associated mutants thereof, pro-SP-C L188Q (mutation in the BRICHOS domain) and pro-SP-C I73T (mutation in the linker region), hereafter referred to as WT BRICHOS, L188Q, and I73T, respectively. We studied protein binding and insertion into biological membranes with different compositions (either in the absence or presence of poly-Val peptides) and how binding and/or insertion affects membrane and protein structural properties. Results show that the co-translational folding of the pro-SP-C poly-Val TM segment is inefficient, suggesting that the presence of the BRICHOS domain is necessary to promote the correct folding of SP-C, and that the BRICHOS domain inserts into superficial parts of the ER membrane.

Experimental Procedures

Recombinant Proteins, Peptides, Enzymes, and Chemicals—WT pro-SP-C BRICHOS (residues 59–197), L188Q, and I73T were expressed and purified as described previously (19, 27), and synthetic peptides were obtained as described by Willander *et al.* (16). The BRICHOS domain of pro-SP-C encompasses residues 90–197, and the linker region corresponds to residues 59–89 (16).

Unless otherwise stated, all chemicals were from Sigma. Plasmid pGEM1, TNT[®] Quick Coupled transcription/translation system, rabbit reticulocyte lysate system, and deoxynucleotides were from Promega (Madison, WI). [³⁵S]Met was from PerkinElmer Life Sciences. All enzymes were from Fermentas (Burlington, Ontario, Canada), except Phusion DNA polymerase, which was from Finnzymes (Espoo, FI) and SP6 RNA Polymerase from Promega. The QuikChange[™] Site-directed Mutagenesis kit was from Stratagene (La Jolla, CA) and oligonucleotides were from Eurofins MWG Operon (Ebersberg, DE). Synthetic 1,2-dipalmitoyl-phosphatidylcholine (DPPC), 1-palmitoyl-2-oleoyl-phosphatidylcholine

(POPC), and 1-palmitoyl-2-oleoyl-phosphatidylglycerol (POPG) were purchased from Avanti Polar Lipids (Birmingham, AL). Organic solvents (chloroform and methanol) used to dissolve lipids were HPLC-grade (Scharlau, Barcelona, Spain). The fluorescent probes 1,6-diphenyl-1,3,5-hexatriene (DPH) and the free radical 2,2,6,6-tetramethyl-1-piperidinyloxy (TEMPO) were purchased from Molecular Probes (Eugene, OR). The detergents octaethylene glycol monododecyl ether ($C_{12}E_8$) and dodecyl- β -D-maltoside (DM) were purchased from Sigma. All other reagents were of analytical grade and obtained from Merck (Darmstadt, Germany).

pGEM1 DNA Manipulations—Full-length WT pro-SP-C (197 residues) was cloned into the pGEM1 vector (Promega) at XbaI/SmaI sites together with a preceding Kozak sequence (28) as previously described (29). The well characterized control protein leader peptidase (Lep) from *Escherichia coli* was cloned into the pGEM1 vector using the same restriction sites as above. To introduce N-linked glycosylation acceptor sites into the gene in the N-terminal part (N5) of the pro-SP-C, Asn⁵-Lys-Thr was substituted for Ser⁵-Lys-Glu. In the C-terminal part (Asn⁶⁵, Asn⁶⁷, Asn⁶⁸, Asn⁶⁹, Asn⁷⁰, and Asn⁷⁸), Asn⁶⁵-Glu-Thr was substituted for Thr⁶⁵-Glu-Met, Asn⁶⁷-Val-Thr was substituted for Met⁶⁷-Val-Leu, Asn⁶⁸-Leu-Thr was substituted for Val⁶⁸-Leu-Glu, Asn⁶⁹-Glu-Thr for Leu⁶⁹-Glu-Met, Asn⁷⁰-Met-Thr for Glu⁷⁰-Met-Ser, and Asn⁷⁸-Gln-Thr for Ala⁷⁸-Gln-Gln. To create spacers of 5 amino acid residues, Ser-Ala-Gln-Gly-Ala was introduced between positions 61 and 62 or 81 and 82. To create the poly-Leu pro-SP-C construct, all valine amino acid residues in the TM segment were changed to leucine residues (19). Site-specific mutagenesis was performed using the QuikChange™ Site-directed Mutagenesis Kit from Stratagene. All mutants were confirmed by sequencing of plasmid DNA at Eurofins MWG Operon (Ebersberg, DE).

Expression in Vitro—All pro-SP-C constructs cloned in the pGEM1 were transcribed and translated in the TNT® SP6 Quick Coupled System from Promega. 150–200 ng of DNA template, 1 μ l of [³⁵S]Met (5 μ Ci), and 0.5 μ l of column-washed dog pancreas rough microsomes (CRMs) (tRNA Probes) (30) were added to 10 μ l of lysate at the start of the reaction, and the samples were incubated for 90 min at 30 °C.

For endoglycosidase H (Endo H) treatment, 6 μ l of the TNT reaction mixture were mixed with 3 μ l of dH₂O and 1 μ l of $\times 10$ glycoprotein denaturing buffer. After addition of 1 μ l of Endo H (500,000 units/ml; New England Biolabs, MA), 7 μ l of dH₂O, and 2 μ l of $\times 10$ G5 reaction buffer, the sample was incubated for 1 h at 37 °C (31).

For proteinase K (PK) treatment, 9 μ l of the TNT reaction mixture were mixed with 1 μ l of 200 mM CaCl₂ and 0.2 μ l of PK (4.5 μ g/ μ l). Next, the sample was incubated for 30 min on ice. At the end of the incubation time, 1 μ l of phenylmethylsulfonyl fluoride (PMSF) (20 μ g/ μ l) was added and incubated for 5 min on ice.

Translation products were analyzed by SDS-polyacrylamide gel electrophoresis, and proteins were visualized in a Fuji FLA-3000 phosphorimager (Fujifilm, Tokyo) using the Image Reader V1.8/Image Gauge version 3.45 software (Fujifilm). The MultiGauge (Fujifilm) software was used to generate a profile of each gel lane, and the multi-Gaussian fit program from the Qti-

plot software package was used to calculate the peak areas of the non-glycosylated and glycosylated protein bands. The glycosylation efficiency of a given glycosylation site was calculated by dividing the area of the single glycosylated band by the summed areas of the glycosylated and non-glycosylated bands. The glycosylation efficiency of the double glycosylation was calculated by dividing the areas of the doubly glycosylated bands by the summed areas of the singly and doubly glycosylated bands. On average, the glycosylation levels vary by no more than $\pm 5\%$ between repeated experiments.

Preparation of Lung Microsomal Membranes—Lung tissue from rat was excised and carefully washed with ice-cold 50 mM Tris-HCl buffer (pH 7.4) containing 0.15 M KCl, 1 mM EDTA, 1 mM dithioerythritol, and 5% glycerol. A 20% homogenate was prepared in the same buffer and the microsomal fraction was obtained as previously described (32). Microsomal pellets were resuspended in the same buffer and resedimented at 150,000 \times g for 45 min. Microsomal membranes were used for lipid extraction and microsomal phospholipids were quantitated by phosphate analysis (32).

Membrane Insertion Experiments—Monolayer experiments were performed at 25 °C using a thermostated Langmuir-Blodgett trough (102 M micro Film Balance, NIMA Technologies, Coventry, United Kingdom) equipped with an injection port and magnetically stirred (33). The trough is equipped with two symmetrical movable barriers controlled by an electronic device. The subphase employed was 5 mM Tris-HCl (pH 7.4) buffer containing 150 mM NaCl. For penetration studies, monolayers were formed by spreading 10 μ l of a concentrated solution of lung microsomal lipids, synthetic phospholipids, or phospholipid/hydrophobic peptide mixtures (50:1, w/w) dissolved in chloroform/methanol (2:1) (v/v) at the air-water interface to give the indicated initial surface pressures (from 5 to 50 mN/m). After organic solvent evaporation, the monolayer was allowed to stabilize for a few minutes before 100 μ l of a stock solution of WT BRICHOS, L188Q, or I73T was injected into the subphase without disturbing the lipid monolayer. Then, protein-induced changes in the monolayer surface pressure at constant surface area were measured. The final protein concentration in the subphase was 18.2 ng/ml (1 nM).

Preparation of Phospholipid Vesicles—Multilamellar vesicles (MLVs) and large unilamellar vesicles (LUVs) were prepared as previously described (34). Briefly, different amounts of DPPC, POPC, or POPG, dissolved in chloroform/methanol (3:1) (v/v), were used alone or mixed to achieve the desired ratios. Then, phospholipids were dried under a N₂ stream and under reduced pressure overnight. MLVs were prepared by hydrating the dry lipid film in 150 mM NaCl, 0.1 mM EDTA, and 5 mM Tris/HCl (pH 7.4) (buffer A), and allowing them to swell for 1 h at a temperature above their T_m . After vortexing, the resulting multilamellar vesicles were used for different assays. LUVs of POPG, POPC, and DPPC/POPG (1:1, w/w) (120 \pm 25 nm) were prepared from the corresponding MLVs at 4 °C (POPC or POPG) and 45 °C (DPPC/POPG) in buffer A with a Mini-Extruder (Avanti Polar Lipids, Birmingham, AL) according to the manufacturer's instructions. For vesicle size analysis, dynamic light scattering was used as described below.

Dynamic Light Scattering—A Zetasizer Nano S (Malvern Instruments, Malvern, UK) equipped with a 633-nm HeNe laser was used for vesicle size analysis and to measure the hydrodynamic diameters of WT BRICHOS, L188Q, and I73T in 20 mM phosphate buffer (pH 7.4) at 25 °C. For each sample, six scans were performed, and all of the samples were analyzed in triplicate. The hydrodynamic diameter was calculated using the General Purpose algorithm available from the Malvern software for dynamic light scattering analysis, which correlates the diffusion coefficient to the hydrodynamic diameter through the Stokes-Einstein equation,

$$d_H = \frac{k_B T}{3 \pi \eta D} \quad (\text{Eq. 1})$$

where k_B is the Boltzmann constant, T is the temperature, η is the viscosity, and D is the translational diffusion coefficient. The Multiple Narrow Modes algorithm was also used to verify the results obtained by the General Purposed method.

To study the dissociation of proteins in the presence of non-denaturing detergents ($C_{12}E_8$ and dodecyl- β -D-maltoside), their hydrodynamic diameters were measured in solution in the presence and absence of increasing concentrations of $C_{12}E_8$ or dodecyl- β -D-maltoside in 20 mM phosphate buffer (pH 7.4).

CD Spectroscopy—Far-UV CD spectra of WT BRICHOS, L188Q, and I73T in the absence and presence of phospholipid vesicles of POPC and POPG were obtained on a Jasco J-715 spectropolarimeter fitted with a 150-watt xenon lamp as previously reported (26). Quartz cells of 1-mm path length were used. Four scans were accumulated and averaged for each spectrum. The acquired spectra were corrected by subtracting the appropriate blank runs (of buffer or phospholipid vesicle solutions), and subjected to noise reduction analysis; data are presented as molar ellipticities (θ) ($\text{kdeg cm}^{-2} \text{dmol}^{-1}$), using 130 Da as the average residue mass. All measurements were performed in 5 mM Tris/HCl buffer (pH 7.4), containing 150 mM NaCl at 25 °C. The protein concentration was 10 μM . Estimation of the secondary structure content from the CD spectra was performed after deconvolution of the spectra into four simple components (α -helix, β -sheet, β -turn, and random coil) according to the convex constraint algorithm (35).

Differential Scanning Calorimetry (DSC)—Calorimetric measurements were performed as previously reported (26, 36, 37) in a Microcal VP differential scanning calorimeter (Microcal Inc., Northampton, MA). To study how WT BRICHOS, L188Q, and I73T affect the thermotropic behavior of phospholipid membranes, MLVs (1 mM) of different phospholipid mixtures (DPPC/POPG (1:1, w/w), DPPC/POPC (1:1, w/w), and DPPC), in the absence and presence of proteins, were loaded in the sample cell of the microcalorimeter with 0.6 ml of 20 mM phosphate buffer (pH 7.4) in the reference cell. All solutions were degassed just before loading into the calorimeter. Three calorimetric scans were collected from each sample between 15 and 95 °C at a heating rate of 0.5 °C min^{-1} . The reversibility of the thermal transition was evaluated by several cycles of heating and cooling. On the other hand, to analyze the effect of detergents or phospholipid vesicles on the WT BRICHOS, L188Q, and I73T thermal unfolding, the proteins were analyzed in the

presence and absence of detergents or phospholipid vesicles with T_m below 0 °C (POPC or POPG). Data were also collected between 20 and 95 °C at a heating rate of 0.5 °C/min. The standard microcal origin software was used for data acquisition and analysis. The excess heat capacity functions were obtained after subtraction of the buffer baseline.

DPH Fluorescence Quenching by TEMPO—DPH fluorescence quenching by TEMPO was carried out as described previously (33). Briefly, lipids, DPH, and TEMPO (when required) were mixed at a 300:1:1 molar ratio (final phospholipid concentration 1 mg/ml). LUVs composed of DPPC/POPG (1:1, w/w) fluorescently labeled with DPH or DPH + TEMPO were then prepared in buffer A as described above, and different amounts of WT BRICHOS or L188Q were added to vesicles. Fluorescence emission of DPH was recorded at 428 nm ($\lambda_{\text{ex}} = 360 \text{ nm}$) at 37 °C, using an SLM-Aminco AB-2 spectrofluorimeter equipped with Glam Prism polarizers and a thermostat-regulated cuvette holder (± 0.1 °C) (Thermo Spectronic, Waltham, MA). Quartz cuvettes of 5 \times 5-mm path length were used.

Results

ER Membrane Targeting and Insertion of Pro-SP-C—Glycosylation assay is an established and well defined method for accurately measuring the glycosylation status of the nascent chain in the ER lumen (4, 31). This approach can be used to determine the topology of membrane proteins (29) and analyze conformational changes in the polypeptide chain (17, 38).

To investigate the targeting and insertion of pro-SP-C into the ER membrane, we introduced *N*-linked glycosylation sites, Asn-Xaa-Thr (NXT), at positions 5 (N5) or 78 (N78) of pro-SP-C. Then, protein expression *in vitro* in the reticulocyte lysate in the absence and presence of pancreatic CRM was performed (Fig. 1, A and B). Dog pancreas microsomes have been widely used for translocation and integration of membrane proteins in the ER, and for glycosylation of acceptor sites by the OST complex (4).

Fig. 1C shows that about 70% of WT pro-SP-C adopted the predicted topology (type II orientation, $N_{\text{cyt}}-C_{\text{lum}}$), whereas about 30% adopted the opposite orientation ($N_{\text{lum}}-C_{\text{cyt}}$). Fig. 1C also shows that pro-SP-C (Leu) with leucine residues in the TM segment, has the same topology distribution as WT pro-SP-C. To exclude the incorrect $N_{\text{lum}}-C_{\text{cyt}}$ orientation and untargeted variants, we kept the acceptor sites N5 and N78 in all the constructs. Glycosylation of pro-SP-C N78 was confirmed by Endo H treatment (Fig. 1D) as a control for the modification of the nascent chain by the OST enzyme. Moreover, as a control of integrity for canine microsomal preparations, a well characterized protein wild-type Lep (normally located in the inner membrane of *Escherichia coli*) was expressed in the presence and absence of CRMs and the translation product was treated with proteinase K (Fig. 1E). We found that the protected fragment migrated at the expected size of the digested control protein, indicating that canine microsomes form tight vesicles. The intactness of microsomal preparations was also assessed by proteinase K treatment of pro-SP-C WT expressed in the presence of CRMs (Fig. 1E).

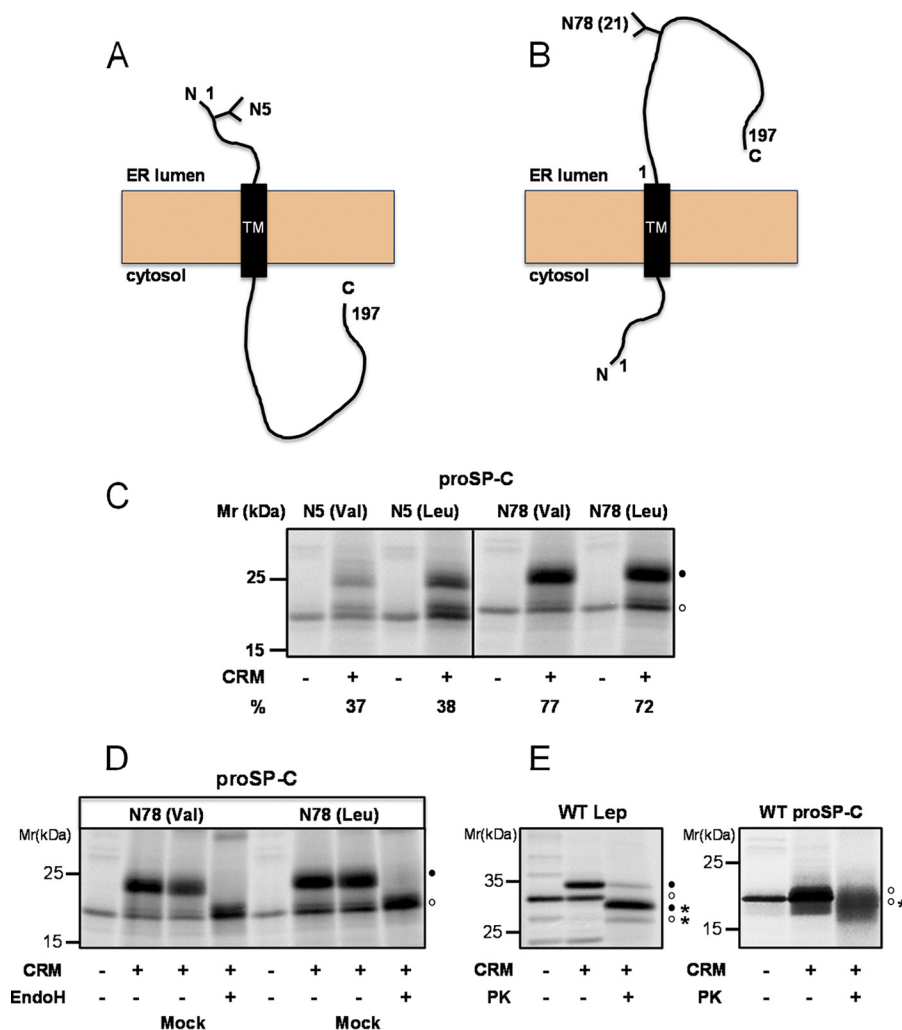


FIGURE 1. Orientation and glycosylation of WT pro-SP-C (Val) and pro-SP-C (Leu). Models of the N_{lum} - C_{cyt} (A) and N_{cyt} - C_{lum} orientation (B) of WT pro-SP-C. The Asn-X-Thr glycosylation acceptor sites (Y) were introduced into the N- (N5) or C-terminal (N78) tails. C, the percentages of glycosylated WT Pro-SP-C (Val) and pro-SP-C (Leu) *in vitro* translated in the presence and absence of dog pancreas rough microsomes (CRMs) are given below as the means of three experiments. D, after Endo H treatment, pro-SP-C migrated as a non-glycosylated product. E, as a control of the integrity of the CRMs, WT pro-SP-C and WT Lep from *E. coli* were expressed in the absence and presence of CRMs and treated with proteinase K (PK), which resulted in fragments that migrated at the expected sizes. The cleaved and protected products are indicated by a star. In C–E, non-glycosylated and glycosylated forms are indicated by unfilled and filled circles, respectively.

Structural Properties of WT Pro-SP-C TM Segment and a Poly-Leu Analog—Using the translocon-mediated *in vitro* assay, we have previously shown that structural properties of TM segments can be mapped by analyzing the glycosylation status of the polypeptide (17, 38). To analyze structural differences between the Val-TM and Leu-TM segment of the nascent chain of pro-SP-C, we determined the N-linked glycosylation status by introducing NXT glycosylation acceptor sites at different distances from the luminal end of the pro-SP-C TM segment.

We have previously determined that the minimal distance between the active site of OST and the luminal end of a TM segment for efficient glycosylation is ~10–12 residues (39, 40). Here, we introduced N-linked glycosylation sites in five different positions (N65, N67, N68, N69, and N70) located at 8 to 13 residues from the luminal end of the pro-SP-C TM segment. Furthermore, two additional sites were introduced in all constructs as control sites: one at position 5 (N5) in the N-terminal and the other at position 78 (N78) in the C-terminal (Fig. 2A).

The efficiency of glycosylation was determined for each construct after translocon-mediated *in vitro* translation in the presence of CRMs.

Our results show that WT pro-SP-C with a glycosylation site at position N65 (8 residues) was only singly glycosylated; however, by moving the glycosylation site residue one at a time until 13 residues (N70) away from the TM segment, the glycosylation efficiency increased from as low as 0% to nearly maximum (64%) (Fig. 2, B and C). The glycosylation profile of poly-Leu pro-SP-C was clearly distinct from that of the WT pro-SP-C (Fig. 2, B and C). When comparing the glycosylation status of WT pro-SP-C (Val) and pro-SP-C (Leu) at roughly the same acceptor site distance, for example, at 12 residues (position N69), we found 41% double glycosylation for WT pro-SP-C (Val) versus 29% double glycosylation for pro-SP-C (Leu). These results indicate that valine residues exhibited a more extended conformation than leucine residues, which adopt a compact conformation in the ribosome-translocon channel (17).

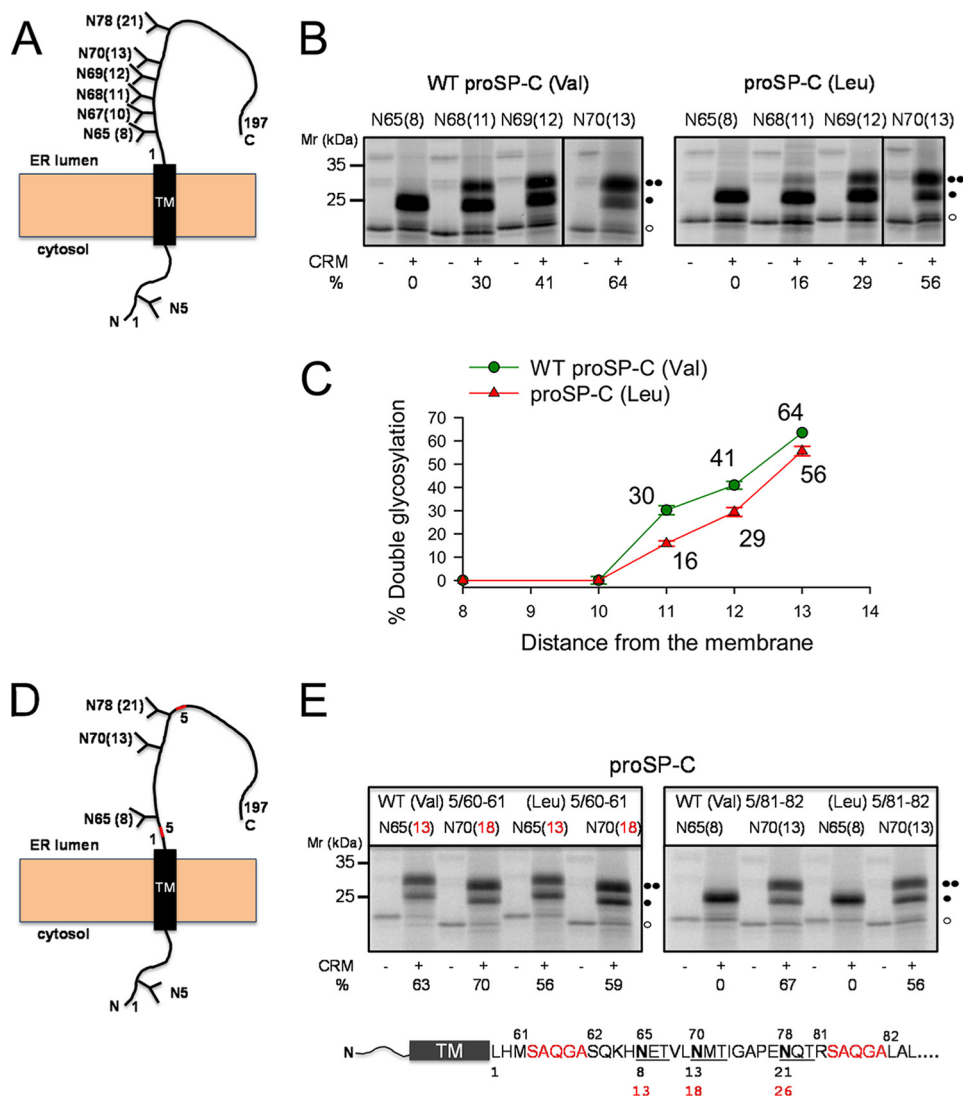


FIGURE 2. Mapping the minimal glycosylation distance for pro-SP-C containing TM segments of WT (Val) and Leu residues. *A*, model of pro-SP-C in an $N_{\text{cyt}}-C_{\text{lum}}$ orientation with Asn-X-Thr glycosylation acceptor sites (Y) introduced into the N-terminal tail (N5) and/or into the C-terminal domain (N65, -68, -69, -70, and -78) at a distance of 8–21 residues from the luminal end of the TM segment. *B*, *in vitro* translation of constructs containing glycosylation sites at different positions (distanced from TM segment within parentheses) of WT pro-SP-C (Val) and pro-SP-C (Leu). The percentage of double glycosylation is given below the lanes. *C*, the percentages of doubly glycosylated Val-TM or Leu-TM segments of pro-SP-C are indicated. Values are mean \pm S.E. of at least three independent experiments. *D*, model of pro-SP-C, with five extra amino acid residues (in red) introduced between positions 61 and 62 or 81 and 82. *E*, addition of five amino acid residues between positions 61 and 62 increases the percentage of double glycosylation for both WT pro-SP-C (Val) and pro-SP-C (Leu). Addition of five amino acid residues between positions 81 and 82 does not affect N65 and N70 glycosylation. In *B* and *E*, non-glycosylated, singly glycosylated, and doubly glycosylated forms of proteins are indicated by one open circle, one filled circle, and two filled circles, respectively.

To further confirm these results, we introduced an extra spacer with five amino acid (Ser-Ala-Gln-Gly-Ala) residues between positions 61 and 62 or 81 and 82 (Fig. 2*D*). The first one (61–62) is located downstream of N65, which moves all the glycosylation sites further away from the membrane. Fig. 2*E* shows that the N65 site increased the percentage of double glycosylation from 0 to 63% for WT pro-SP-C (Val) and from 0 to 56% for pro-SP-C (Leu). In addition, at a distance of 18 residues (N70 position) from the membrane, the percentage of double glycosylation was 70% for WT pro-SP-C (Val) and 59% for pro-SP-C (Leu). These results are consistent with the fact that both sites (N65 and N70) were moved 5 residues away from the TM luminal end of pro-SP-C. As expected, the second spacer located upstream of all the glycosylation sites (81–82) did not affect the glycosylation efficiencies (Fig. 2*E*).

WT BRICHOS, but Not ILD-associated Mutants, Inserts into the Membrane Surface—We have previously reported that pro-SP-C BRICHOS binds to phospholipid vesicles of POPC with a K_D of $6.2 \pm 0.8 \mu\text{M}$ (26). To analyze insertion of recombinant WT BRICHOS, L188Q, and I73T into phospholipid membranes, we measured the surface pressure increase induced by the insertion of these proteins into monolayers (Fig. 3). To perform these experiments, we used monolayers composed of ER lipids or synthetic phospholipids (POPC, DPPC, or DPPC/POPC in a 1:1 weight ratio).

The injection of WT BRICHOS, L188Q, or I73T into the aqueous subphase (1 nM, final concentration) beneath the lipid monolayer resulted in a rapid increase in the monolayer surface pressure to a steady-state value called the equilibrium adsorption pressure (π_e), which depended on the initial monolayer

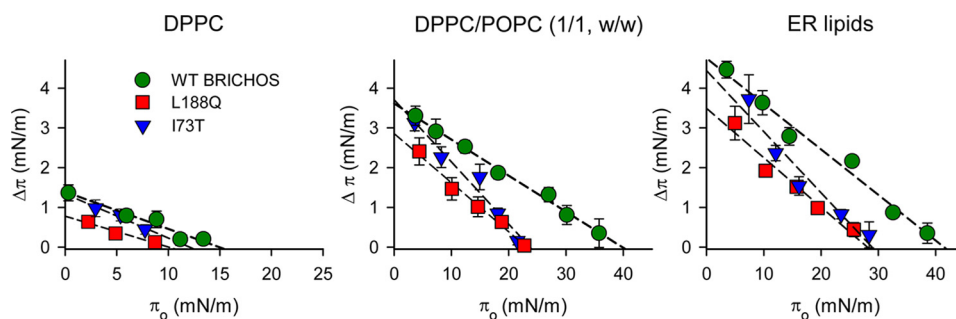


FIGURE 3. **WT BRICHOS, but not ILD-associated mutants, insert into the membrane surface.** Surface pressure increase induced by the insertion of WT BRICHOS, L188Q, and I73T into DPPC, DPPC/POPC (1:1, w/w), and ER lipid monolayers as a function of the initial surface pressure. The straight line was obtained by linear regression. The final concentration of WT BRICHOS, L188Q, or I73T in the subphase was 18.2 ng/ml. Values are the mean \pm S.D. of three experiments.

surface pressure (π_0). By plotting the surface pressure increase induced by the insertion ($\Delta\pi = \pi_e - \pi_0$) as a function of initial surface pressure (π_0) of the phospholipid monolayer, the maximum insertion pressure (MIP) of WT BRICHOS, L188Q, and I73T was determined by extrapolation of the regression line to a surface pressure increase equal to zero (Fig. 3). This parameter corresponds to the initial surface pressure of the phospholipid monolayer above which no more protein molecules can penetrate the lipid film and increase surface pressure. Because the membrane lateral pressure has been estimated to be in the range of ~ 30 mN/m, proteins with a MIP below this value cannot penetrate cellular or subcellular membranes (41, 42).

Our results show that WT BRICHOS can penetrate monolayers composed of lung ER lipids (MIP value of 42 ± 0.4). Similar results were found with POPC monolayers (data not shown), which show a single liquid-expanded state (a disordered fluid phase). However, WT BRICHOS cannot insert in DPPC monolayers (MIP value of 14.5 ± 1.5 mN/m). This is because at π of ~ 21 mN/m, pure DPPC monolayers consist of a homogeneous liquid-condensed phase, which is a semicrystalline solid phase (43). Interestingly, WT BRICHOS penetrates DPPC/POPC monolayers, which show a liquid-expanded/liquid-condensed phase coexistence at 30 mN/m (MIP value of 40 ± 0.5 mN/m). Thus, our results indicate that WT BRICHOS is able to insert in loosely packed membranes such as ER or POPC membranes or membranes with coexisting ordered/disordered domains (DPPC/POPC), but not in tightly packed and ordered membranes (DPPC).

The $\Delta\pi_{\max}$ value for ER and DPPC/POPC membranes (4.5 ± 0.1 and 3.9 ± 0.1 mN/m, respectively), obtained by extrapolating the regression of the plot to the y axis, suggest that WT BRICHOS only penetrates superficially in the lipid monolayer in comparison with other proteins (33). A previous study indicated that pro-SP-C BRICHOS does not bind to surfactant phospholipids when a centrifugation assay is used (27). The discrepancy between this finding and our present results can probably be explained by the less sensitive method and the somewhat different phospholipid composition previously used (27) for analysis of BRICHOS binding.

On the other hand, ILD mutants (L188Q and I73T) showed MIP values for DPPC, DPPC/POPC, and ER membranes that are smaller than 30 mN/m (Fig. 3), *i.e.* below the estimated lateral pressure for biological membranes. This indicates that neither L188Q nor I73T would penetrate into the membrane to

any significant extent. In contrast, we found that partial removal of the linker region of WT BRICHOS by trypsin treatment did not affect the insertion of the protein into phospholipid monolayers (data not shown).

Fig. 4 shows that the insertion of WT BRICHOS into mixed monolayers of DPPC/POPC (1:1, w/w) significantly increased when the monolayer contained hydrophobic poly-Val peptides (KKV5KK or KKV7KK) (MIP = 45.5 ± 1.2 mN/m; $\Delta\pi_{\max} = 6.9 \pm 0.4$ mN/m), but not SP-CLeu in a helical conformation (MIP = 33.6 ± 0.4 mN/m; $\Delta\pi_{\max} = 3.7 \pm 0.3$ mN/m). Thus, the presence of hydrophobic non-helical poly-Val peptides in the phospholipid monolayer promoted partial WT BRICHOS insertion into the membrane, as demonstrated by an increase in both MIP and $\Delta\pi_{\max}$ values.

In contrast, L188Q and I73T mutants were unable to insert into DPPC/POPC membranes (1:1, w/w) in either the absence or presence of poly-Val peptides (MIP = 23 ± 2). The fact that L188Q and I73T mutants were unable to insert into ER or DPPC/POPC membranes argues that the anti-amyloid activity of the WT BRICHOS domain might be related to its ability to partly penetrate biological membranes and recognize a nonhelical segment of hydrophobic amino acid residues of unfolded pro-SP-C.

WT BRICHOS, but Not ILD-associated Mutants, Dissociates in the Presence of Detergents—We have previously shown that recombinant WT BRICHOS mainly forms trimers in solution and in the crystal structure (16, 26). However, peptide-binding experiments indicate that peptide substrates bind to monomeric BRICHOS domains (44, 45). Hence, the active form of WT BRICHOS appears to be the monomer. To find out whether WT BRICHOS trimers dissociate to the monomeric functional form after lipid interaction, we studied the hydrodynamic size of WT BRICHOS particles in the absence and presence of non-denaturing detergents, such as $C_{12}E_8$ and dodecyl- β -D-maltoside.

Dynamic light scattering analysis of WT BRICHOS indicates that, in the absence of detergents, the protein exhibited a unique peak, which corresponds to particles with a hydrodynamic diameter of 9.6 ± 0.8 nm (Fig. 5A). Addition of increasing concentrations of $C_{12}E_8$ ranging from 0 to 0.185 mM to a WT BRICHOS solution (10 μ M) caused a detergent concentration-dependent decrease of WT BRICHOS size. At detergent concentrations higher to CMC $_{C_{12}E_8}$ (0.11 mM), only one peak was observed with a hydrodynamic diameter of $4.5 \pm$

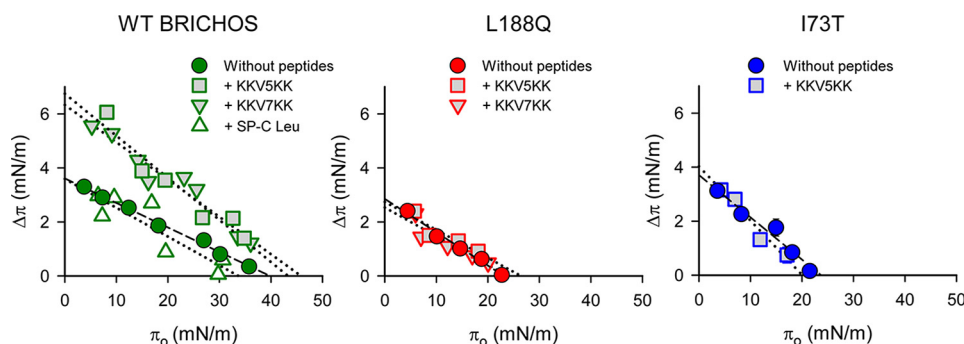


FIGURE 4. **The presence of hydrophobic non-helical poly-Val peptides in the phospholipid monolayer promotes WT BRICHOS insertion.** Surface pressure increase induced by the insertion of WT BRICHOS, L188Q, or I73T into DPPC/POPC (1:1, w/w) monolayers with or without different peptides as a function of the initial surface pressure. The phospholipid/peptide weight ratio was 50:1. Values are the mean of three experiments.

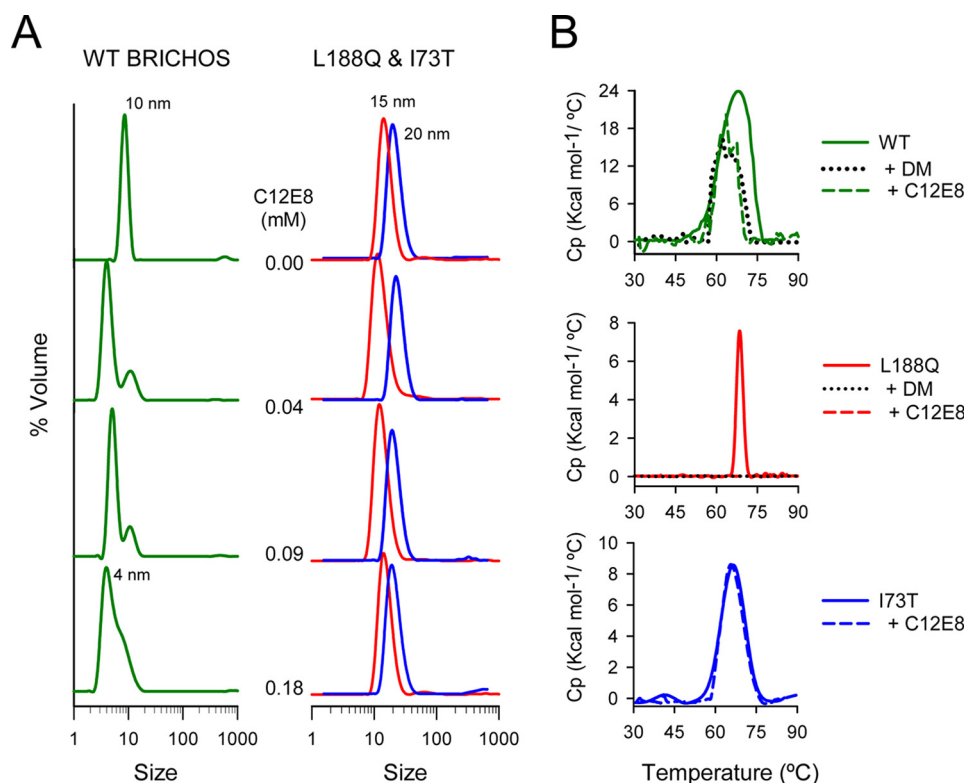


FIGURE 5. **Hydrodynamic diameter (A) and thermal stability (B) of free and detergent-bound WT BRICHOS, L188Q, and I73T.** A, DLS analysis of the hydrodynamic diameter of WT BRICHOS (10 nm), L188Q (15 nm), and I73T (20 nm) in the absence and presence of increasing concentrations of $C_{12}E_8$. The y axis represents the relative intensity of the scattered light, and the x axis denotes the hydrodynamic diameter of the particles present in the solution. The concentrations of WT BRICHOS and L188Q were $10 \mu\text{M}$. Similar results were found with dodecyl- β -D-maltoside. B, thermal unfolding of WT BRICHOS (10 μM), L188Q (10 μM), and I73T (10 μM) in the absence and presence of $C_{12}E_8$ (0.15 mM) or dodecyl- β -D-maltoside (0.15 mM). Similar results were found in the presence of POPC multilamellar vesicles (phospholipid to protein weight 10:1). In A and B, one representative experiment of three is shown.

0.3 nm, which presumably consists of a dissociated, monomeric form of WT BRICHOS. Similar results were found with DM. Neither $C_{12}E_8$ nor DM were detectable by DLS at concentrations lower or equal to their CMC. These studies were performed with polyoxyethylene glycol and non-ionic detergents instead of unilamellar phospholipid vesicles (LUVs), because LUVs scatter much more light than WT BRICHOS particles and might mask small protein particles.

Fig. 5A also shows that the hydrodynamic diameter of L188Q (14.7 ± 1 nm) and I73T (20 ± 2.3 nm) particles in the absence of detergents was greater than that of WT BRICHOS particles, indicating that the degree of oligomerization or multimerization of L188Q and I73T was higher than that of WT BRICHOS.

In addition, Fig. 5A shows that the interaction of L188Q (10 μM) or I73T (10 μM) with increasing concentrations of $C_{12}E_8$ (or DM) did not cause any change in the hydrodynamic diameter of L188Q or I73T particles.

DSC was used to determine thermal stability of free and detergent-bound proteins. Fig. 5B shows the melting curves of WT BRICHOS and ILD-associated mutants (L188Q and I73T) in the absence and presence of detergents ($C_{12}E_8$ or DM). In the absence of detergents, the melting curve of WT BRICHOS, L188Q, and I73T displayed one heat absorption peak over a temperature range of 30–90 °C. The apparent T_m values were 66.4 ± 0.4 °C for WT BRICHOS, 68 ± 0.8 °C for L188Q, and 65.3 ± 0.5 °C for I73T ($n = 3$). DSC revealed that the thermal

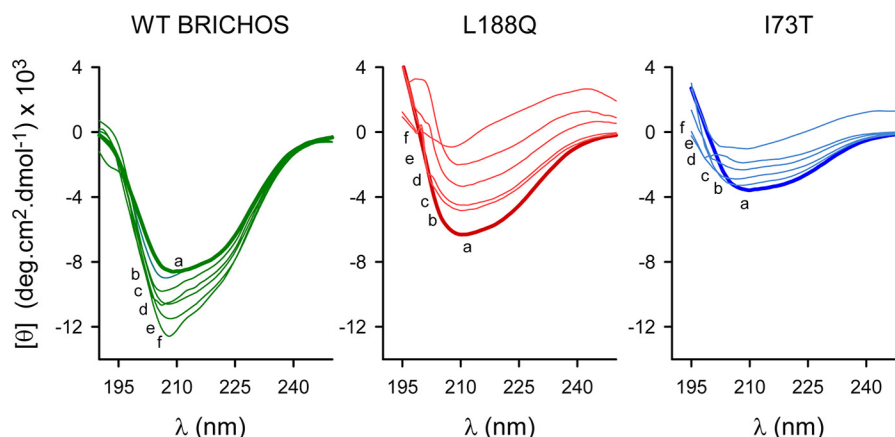


FIGURE 6. **Binding of WT BRICHOS, L188Q, and I73T to membranes results in changes in protein secondary structure.** Changes in the circular dichroic spectrum of WT BRICHOS, L188Q, or I73T as a function of POPC/protein weight ratio: (a) no phospholipid; (b) 0.25:1; (c) 1:1; (d) 5:1; (e) 10:1; (f) and 20:1. LUVs of 100–130 nm were used. The protein concentration was 182 $\mu\text{g}/\text{ml}$.

unfolding of L188Q was more cooperative than that of WT BRICHOS and I73T mutant and that it was not reversible after heating to 100 °C (data not shown). These data also suggest structural differences between the L188Q and I73T mutants. Fig. 5B also shows that $C_{12}E_8$ - or DM-bound WT BRICHOS displayed two transitions with maxima at 62 and 67 °C. The first, second, and third heat capacity curves of $C_{12}E_8$ - or DM-bound WT BRICHOS overlapped (data not shown). Similar results were found with POPC vesicle-bound WT BRICHOS (26). These results suggest that the low temperature endotherm might correspond to monomers and the high temperature endotherm to trimers or higher oligomers. Thus, it is possible that the binding of WT BRICHOS to lipid vesicles or detergent micelles causes trimer destabilization and/or monomer stabilization.

In contrast, the presence of $C_{12}E_8$ did not affect the I73T thermogram, and L188Q binding to micelles resulted in the disappearance of the heat absorption peak over a temperature range of 15–100 °C. Similar results were found in the presence of POPC vesicles (data not shown), indicating that binding of L188Q, but not I73T, to phospholipid membranes or detergent micelles causes an alteration of the L188Q conformation, with unfolding likely occurring at temperatures higher than those now studied. Further studies are required to understand the molecular mechanisms by which micelles or lipid vesicles affect the thermal unfolding of the L188Q, but not the I73T, mutant.

Binding of WT BRICHOS and ILD-associated Mutants to Membranes Results in Changes in Protein Secondary Structure—We used CD spectroscopy to determine whether membrane binding alters the secondary structure of these proteins (Fig. 6). As previously reported (26), in the absence of lipids, WT BRICHOS was characterized by 32% α -helix, 34% β -sheet, 15% β -turn, and about 20% random coil structures (Table 1). The binding of WT BRICHOS to POPC unilamellar vesicles modified the CD signal. The negative ellipticity increased with increasing concentrations of POPC, and the minimum was progressively blue-shifted (Fig. 6). The percentage of α -helix and β -sheet structures significantly decreased, whereas that of the random coil structure increased in membrane-bound WT BRICHOS (Table 1).

On the other hand, L188Q was characterized by 20% α -helix, 50% β -structures, and about 30% random coil structures, in the absence of lipids, whereas I73T showed about 10% α -helix, 75% β -structures, and about 15% random coil structures. Membrane-bound L188Q and I73T showed a significant decrease in α -helix structure and a parallel increase in β -structures, whereas that of the random coil structure did not change (Fig. 6B, Table 1).

WT BRICHOS, but Not ILD-associated Mutants, Affects the Lipid Acyl Chain Packing of Membranes with Coexisting Ordered/Disordered Domains—DSC is a valuable tool to study the ability of exogenously added proteins to interact with lipid membranes and affect the lipid acyl chain packing. Fig. 7 shows the effect of WT BRICHOS and L188Q on DSC heating scans of DPPC ($T_m = 41.5 \pm 0.1$), DPPC/POPG (1:1, w/w) ($T_m = 26.0 \pm 0.3$), and DPPC/POPC (1:1, w/w) ($T_m = 29.5 \pm 0.3$) multilamellar vesicles.

Fig. 7 shows that the thermal transition of mixed membranes composed of DPPC/POPG (1:1, w/w) or DPPC/POPC (1:1, w/w) exhibited a broader melting event with lower melting enthalpy (ΔH) compared with DPPC membranes, due to the presence of low T_m phospholipids (POPC or POPG) in these membranes. WT BRICHOS, but not L188Q, significantly increased the enthalpy of the thermal transition of DPPC/POPG ($\Delta H = 4.0 \pm 0.5$ kcal/mol versus $\Delta H_{\text{BRICHOS}} = 6.1 \pm 0.6$ kcal/mol, $p < 0.01$) and DPPC/POPC ($\Delta H = 3.7 \pm 0.6$ kcal/mol versus $\Delta H_{\text{BRICHOS}} = 5.5 \pm 0.2$ kcal/mol, $p < 0.05$), but not that of DPPC membranes. In addition, WT BRICHOS, but not L188Q and I73T, produced a significant increase in the T_m of acidic phospholipid vesicles (DPPC/POPG) ($T_m = 26.0 \pm 0.3$ °C versus $T_{mB} = 27.4 \pm 0.1$ °C, $p < 0.05$), which is consistent with an electrostatic, charge-neutralization interaction of WT BRICHOS (pI 5.75) at the bilayer surface, which would condense and stabilize the gel state phospholipid bilayer. Moreover, WT BRICHOS-induced increase of ΔH might be explained by a protein-induced increase of van der Waals interactions between lipid acyl chains after protein adsorption and partial insertion into the membrane surface.

To confirm that the interaction and partial insertion of WT BRICHOS into the membrane surface produces increased lipid

TABLE 1

Secondary structure of WT BRICHOS, L188Q, and I73T in the absence and presence of phospholipid vesicles

The phospholipid to protein weight ratio was 10:1.

	% Secondary structure			
	α -Helix	β -Sheet	β -Turn	Random
WT BRICHOS	32 \pm 2	34 \pm 2	15 \pm 1.2	19 \pm 1.8
+ POPC	26 \pm 1.7 ^a	20 \pm 1.8 ^a	15 \pm 1.2	39 \pm 1.8 ^a
+ POPG	27 \pm 1.9 ^a	24 \pm 2.2 ^a	15 \pm 0.8	34 \pm 0.8 ^a
L188Q	20 \pm 1.4	17 \pm 0.8	34 \pm 1.2	29 \pm 1.8
+ POPC	9 \pm 1.4 ^a	26 \pm 1.2 ^a	41 \pm 1.4 ^a	24 \pm 2.8
+ POPG	8 \pm 0.8 ^a	22 \pm 1.6 ^a	40 \pm 1.3 ^a	30 \pm 1.7
I73T	10 \pm 2.1	48 \pm 1.8	26 \pm 1.2	16 \pm 0.6
+ POPC	3 \pm 1.6 ^a	55 \pm 2.2 ^a	27 \pm 1.9	15 \pm 1.2
+ POPG	6 \pm 1.2 ^a	52 \pm 1.6 ^a	28 \pm 0.9	14 \pm 0.6

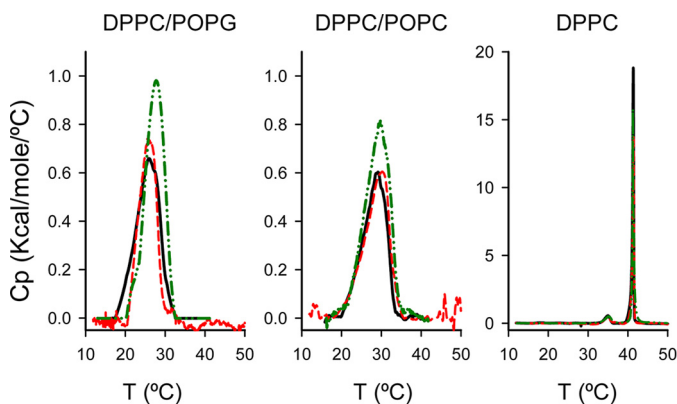
^a $p < 0.05$ vs protein in the absence of lipid vesicles ($n = 3$).

FIGURE 7. WT BRICHOS, but not ILD-associated mutants, increases the phase transition enthalpy of either DPPC/POPG or DPPC/POPC multilamellar vesicles. DSC heating scans of 1 mM DPPC/POPG (1:1, w/w) and DPPC/POPC (1:1, w/w), and DPPC multilamellar vesicles were performed in the absence (black line) and presence of 10 weight % WT BRICHOS (dash-dot-dot line) or 10 weight % L188Q (broken red line). Calorimetric scans were performed at a rate of 0.5 °C/min. Three consecutive scans were recorded for each sample. ILD-associated I73T mutant has the same behavior as the L188Q mutant (data not shown for clarity of presentation). For each figure, one representative experiment of three is shown.

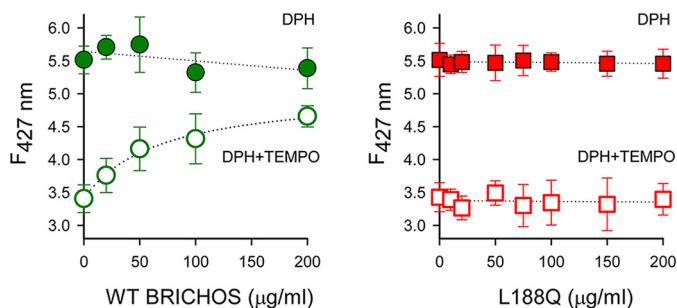


FIGURE 8. WT BRICHOS, but not L188Q, has an ordering effect on DPPC/POPG membranes, decreasing DPH susceptibility to be quenched by TEMPO. DPPC/POPG unilamellar vesicles (1 mg/ml) containing DPH with or without TEMPO were incubated with increasing concentrations of WT BRICHOS or L188Q. F is the emission intensity of DPH at 427 nm in the absence and presence of proteins. Values are the mean \pm S.D. of three experiments.

packing, we analyzed whether WT BRICHOS had any effect on the quenching of DPH fluorescence by the stable radical TEMPO embedded in membranes with coexisting ordered/disordered domains (Fig. 8). The fluorescent probe DPH is known to distribute uniformly over either fluid or solid domains in the membrane, whereas TEMPO partitions only into fluid domains. In DPPC/POPG (1:1, w/w) membranes, with ordered/disordered phase coexistence, TEMPO is able to quench the fluorescence emission of DPH that partitions into

fluid but not solid domains. Fig. 8 shows that addition of increasing WT BRICHOS concentrations to DPPC/POPG vesicles caused an increase of DPH fluorescence in DPPC/POPG vesicles containing TEMPO, but not in those vesicles without TEMPO. These results indicate that WT BRICHOS has an ordering effect on DPPC/POPG membranes, decreasing DPH susceptibility to be quenched by TEMPO. On the other hand, L188Q did not have any effect on DPH fluorescence in the absence or presence of TEMPO, which together with DSC experiments indicates that L188Q has no effect on the lipid acyl chain packing of membranes.

Discussion

It has been found that the formation of TM helices can occur already in the ribosome, possibly mediated by hydrophobic interactions between the TM segment and ribosome components (46). However, this mechanism does not apply to an artificial poly-Val segment that is incapable of forming a compact helical conformation either in the ribosome or in the ER translocon (17). Such a tendency was also observed in our study of distance-dependent glycosylation efficiency in pro-SP-C (Fig. 2). By moving the glycosylation site further from the TM segment, different glycosylation efficiencies in WT pro-SP-C (Val) and pro-SP-C (Leu) could be observed. The fact that the WT protein shows a higher percentage of glycosylated species indicates that it adopts a more extended and unfolded conformation compared with the Leu protein, which needs additional residues to be fully glycosylated because of its more compact and folded conformation.

Pro-SP-C BRICHOS interacts preferably with misfolded, non-helical SP-C, prevents SP-C fibril formation *in vitro*, and inhibits aggregation of mutant pro-SP-C L188Q as amyloid-like inclusions in human embryonic kidney 293 cells (19, 20, 27). Moreover, mutations in the BRICHOS domain of pro-SP-C are associated with proprotein aggregation and/or misprocessing, and lung disease (47, 48). However, the L188Q BRICHOS mutation in pro-SP-C does not give rise to amyloid-like inclusions if the poly-Val TM segment is replaced with poly-Leu (19), strongly suggesting that the inherently high tendency of the poly-Val segment to form β -sheet aggregates contributes to disease related to L188Q mutation.

It is known that there are membrane-integrated chaperones that work specifically on TM regions and prevent their aggregation by binding to polar parts of certain TM helices

BRICHOS-Membrane Interactions

(49, 50). However, pro-SP-C BRICHOS differs from these chaperones by acting upstream of TM helix formation and not being integrated into the membrane but located on the luminal side of the ER membrane. The mechanism by which the water-soluble BRICHOS domain interacts with the hydrophobic pro-SP-C TM segment in the membrane, preventing misfolding of the TM segment, is still unknown. For that reason, we have investigated the interaction of membranes with the recombinant human WT pro-SP-C BRICHOS domain (WT BRICHOS) and two ILD-associated mutants (L188Q and I73T).

The present study shows for the first time that WT BRICHOS, but not two different ILD-associated mutants, with mutations located in the linker region (I73T mutant) or the BRICHOS domain (L188Q mutant), partially inserts into phospholipid membranes (Figs. 3 and 4) and affects membrane physical properties (Figs. 7 and 8). The MIP value obtained for the interaction of WT BRICHOS with loosely packed ER membranes (MIP = 42 ± 0.4 mN/m) or membranes with coexisting ordered/disordered domains (DPPC/POPC) (MIP = 40 ± 0.5 mN/m) is higher than the estimated equilibrium lateral pressure (30 mN/m) for biomembranes (41). These values are in the range of the estimated MIP values for peripheral or amphitropic proteins that insert into membranes to carry out their biological activity (antimicrobial peptides, lipoproteins, lipases, etc.) or pathological activity (amyloid polypeptides, C reactive protein, or Ebola virus matrix protein) (33, 51–53). WT BRICHOS does not insert into DPPC monolayers (MIP = 14.5 ± 1.5 mN/m), which at 17 mN/m consist of a homogeneous solid phase.

The insertion isotherms do not reveal to what extent WT BRICHOS inserts into the membranes. However, given the moderated $\Delta\pi_{\max}$ value of WT BRICHOS insertion in comparison to other proteins or peptides (33, 51–53) and the kind of effects that WT BRICHOS has on the membrane structure (Figs. 7 and 8), we suggest that WT BRICHOS would insert into the headgroup region but not the hydrophobic portion of the membrane. This would facilitate the sensing of conformational changes in the TM part of pro-SP-C and prevent misfolding of the non-helical polyvaline segment of pro-SP-C. Interestingly, the presence of non-helical poly-Val peptides in the DPPC/POPC monolayer promoted insertion into the membrane of WT BRICHOS, but not ILD-associated mutants (I73T and L188Q), as demonstrated by a significant increase in both MIP and $\Delta\pi_{\max}$ values (Fig. 4).

ILD is associated with several different mutations in pro-SP-C. The underlying molecular pathogenic events likely differ among different mutations and are far from being well understood. Different mutations give rise to different disease phenotypes, including age of onset, histopathological characteristics, and severity of disease. Moreover, one and the same mutation can give rise to pleiotropic manifestations (54). In addition, different pro-SP-C mutations result in very varying effects at the cellular level. The first mutation described, Δ exon4, which deletes the last 37 residues of the BRICHOS domain (48), causes a severely toxic phenotype with trapping of the proprotein in the ER, triggering of the unfolded protein response, and rapid degradation by the

proteasomal system (25, 55). Pro-SP-C L188Q, also in the BRICHOS domain, gives rise to alveolar type II cell toxicity, aberrant subcellular localization, and diffuse intracellular protein accumulation (47), whereas the non-BRICHOS I73T mutation results in pro-SP-C misprocessing, dysregulated targeting with proprotein ending up in the plasma membrane as well as in endosomes. The I73T mutation also has effects on surfactant lipid composition (56, 57). Interestingly, amyloid deposits were found in patient lung tissue with either the non-BRICHOS mutation I73T or the BRICHOS mutation Δ 91–93 (the BRICHOS domain encompasses residues 90–197) (16), suggesting that apparently different cellular and molecular mechanisms can result in SP-C amyloid formation.

The present study adds biochemical data showing that both the L188Q and I73T mutations result in recombinant pro-SP-C BRICHOS proteins that, in contrast to the WT counterpart, are unable to insert into loosely packed ER membranes. Apparently, both mutations, within (L188Q) and outside (I73T) the BRICHOS domain, impede membrane insertion. It was proposed that the linker region (where the I73T mutation is localized) and the BRICHOS domain both interact with target peptides (16), but further studies are required to unravel the molecular mechanisms underlying these effects. These observations strengthen the hypothesis that the insertion of pro-SP-C BRICHOS into the ER membrane is necessary for its anti-amyloidogenic activity. Analysis of further pro-SP-C BRICHOS and non-BRICHOS mutants in terms of membrane interactions is warranted to find out to what extent the inability to penetrate into membranes is associated with pro-SP-C mutations. However, it should be pointed out that introducing mutations in pro-SP-C could also affect the folding and stability of the protein, with possible secondary effects on aggregation. In our experience, introducing the mutations T93R, S95R, T93R/S95R or D105N in the pro-SP-C BRICHOS construct used herein give rise to pronounced aggregation and precipitation of the recombinant protein. As a result, these mutants are difficult to handle and yield small amounts of soluble protein (44).⁵ The L188Q mutation results in formation of larger oligomers (Fig. 5), which, however, are soluble and can be studied. This observation is in line with the finding that pro-SP-C-L188Q expressed in cell lines gives rise to the aggregated protein but also to a fraction that is localized to the endolysosomal pathway and is processed to mature SP-C (25).

Whereas the active form of WT BRICHOS has been reported to be the monomer (44, 45), WT BRICHOS mainly forms trimers in solution (16). To find out whether WT BRICHOS undergoes partial structural rearrangements upon binding to lipids that might lead to the formation of monomers, we analyzed the hydrodynamic diameter of the protein in the absence and presence of non-denaturing detergents, such as $C_{12}E_8$ and dodecyl- β -D-maltoside, which mimic the membranous environment (Fig. 5A). We found that trimeric WT BRICHOS, with a hydrodynamic diameter of 9.6 ± 0.8 nm, is able to dissociate into smaller particles of 4.5 ± 0.3 nm

⁵ J. Presto and J. Johansson, unpublished observations.

in the presence of $C_{12}E_8$ or dodecyl- β -D-maltoside. In contrast, the ILD-associated mutants L188Q and I73T are unable to dissociate into monomers upon binding to lipids. The ability to dissociate in the presence of membranes is similar to that observed for other proteins such as pentameric C-reactive protein, whose insertion in cellular membranes (MIP = 33 mN/m) leads to the formation of monomeric CRP (52, 58). This supports the suggestion by Willander *et al.* (16) that the formation of a trimeric BRICHOS is a “capping” mechanism that blocks the putative binding site in the absence of substrate (or membrane), as observed for other molecular chaperones (59, 60).

The lack of capability of ILD-associated mutants (L188Q and I73T) to insert into the membrane surface could be related to their inability to dissociate into monomers upon binding to amphipathic lipids. The different mode of interaction that WT BRICHOS and ILD-associated mutants exhibit with membranes is also manifested in the effects that protein/lipid interaction has on protein and membrane structure. The binding of WT BRICHOS to membranes results in a structurally less ordered protein (Fig. 6). These changes may facilitate insertion of the BRICHOS domain into ER membranes and binding to misfolded pro-SP-C. In contrast, the binding of L188Q or I73T to membranes results in a structurally more ordered protein (Fig. 6), showing a significant increase in β -structures, which might explain the different behavior of ILD-associated mutants upon membrane binding.

With respect to the effect of protein/lipid interaction on membrane physical properties, we found that insertion of WT BRICHOS, but not of L188Q and I73T, into the membrane surface induces a significant increase in the enthalpy of the thermal transition of DPPC/POPC or DPPC/POPG membranes (Fig. 7). These results might be explained by a protein-induced increase of van der Waals interactions between lipid acyl chains after protein adsorption and partial insertion into the membrane surface. The results are consistent with the behavior of peripheral proteins that do not penetrate deeply the hydrophilic-hydrophobic interface of the bilayer (61). Consistent with DSC analysis, we found that insertion of WT BRICHOS, but not of L188Q or I73T, into DPPC/POPG membranes decrease the susceptibility of DPH fluorescence to quenching by TEMPO (Fig. 8), a stable nitroxyl free radical that partitions only into fluid domains. These results indicate that WT BRICHOS occupies some space in the membrane surface, or at least interacts with the membrane surface sufficiently to increase lipid packing, which would help to prevent α -helix to β -sheet conformational changes.

In summary, we have shown that the pro-SP-C TM segment in its process of cotranslational integration into the ER membrane has difficulties in folding correctly and that it may need assistance from the chaperone-like BRICHOS domain to form an α -helix. Furthermore, pro-SP-C BRICHOS needs to be inserted into the membrane surface to interact with misfolded protein, and the BRICHOS-induced lipid packing increase would facilitate its role as a molecular chaperone. The efficiency, specific mechanism, small size, and natural occurrence suggest that the BRICHOS domain

could give important insights into natural anti-amyloid strategies and be used in developing compounds that prevent amyloid diseases.

Author Contributions—A. S. designed, performed, and analyzed experiments, and wrote the first draft of the manuscript. J. P. designed, performed, and analyzed experiments. P. L., L. A. O., and B. G. F. performed and analyzed experiments. I. N. designed and analyzed experiments. J. J. and C. C. designed and coordinated the study, analyzed data, and wrote the paper. All authors reviewed the results and approved the final version of the manuscript.

Acknowledgment—We gratefully thank Prof. Arthur E. Johnson, Texas A&M University, for providing dog pancreas microsomes.

References

- Casals, C., and Cañadas, O. (2012) Role of lipid ordered/disordered phase coexistence in pulmonary surfactant function. *Biochim. Biophys. Acta* **1818**, 2550–2562
- Whitsett, J. A., and Weaver, T. E. (2002) Hydrophobic surfactant proteins in lung function and disease. *N. Engl. J. Med.* **347**, 2141–2148
- Keller, A., Eistetter, H. R., Voss, T., and Schäfer, K. P. (1991) The pulmonary surfactant protein C (SP-C) precursor is a type II transmembrane protein. *Biochem. J.* **277**, 493–499
- Hessa, T., Kim, H., Bihlmaier, K., Lundin, C., Boekel, J., Andersson, H., Nilsson, I., White, S. H., and von Heijne, G. (2005) Recognition of transmembrane helices by the endoplasmic reticulum translocon. *Nature* **433**, 377–381
- Nyathi, Y., Wilkinson, B. M., and Pool, M. R. (2013) Co-translational targeting and translocation of proteins to the endoplasmic reticulum. *Biochim. Biophys. Acta* **1833**, 2392–2402
- Rapoport, T. A. (2007) Protein translocation across the eukaryotic endoplasmic reticulum and bacterial plasma membranes. *Nature* **450**, 663–669
- Shao, S., and Hegde, R. S. (2011) Membrane protein insertion at the endoplasmic reticulum. *Annu. Rev. Cell Dev. Biol.* **27**, 25–56
- Kelleher, D. J., and Gilmore, R. (2006) An evolving view of the eukaryotic oligosaccharyltransferase. *Glycobiology* **16**, 47R–62R
- Hedlund, J., Johansson, J., and Persson, B. (2009) BRICHOS—a superfamily of multidomain proteins with diverse functions. *BMC Res. Notes* **2**, 180
- Sánchez-Pulido, L., Devos, D., and Valencia, A. (2002) BRICHOS: a conserved domain in proteins associated with dementia, respiratory distress and cancer. *Trends Biochem. Sci.* **27**, 329–332
- Sipe, J. D., Benson, M. D., Buxbaum, J. N., Ikeda, S., Merlini, G., Saraiva, M. J., Westermark, P., and Nomenclature Committee of the International Society of Amyloidosis. (2012) Amyloid fibril protein nomenclature: 2012 recommendations from the Nomenclature Committee of the International Society of Amyloidosis. *Amyloid* **19**, 167–170
- Dluhy, R. A., Shanmukh, S., Leopard, J. B., Krüger, P., and Baatz, J. E. (2003) Deacylated pulmonary surfactant protein SP-C transforms from α -helical to amyloid fibril structure via a pH-dependent mechanism: an infrared structural investigation. *Biophys. J.* **85**, 2417–2429
- Gustafsson, M., Thyberg, J., Näslund, J., Eliasson, E., and Johansson, J. (1999) Amyloid fibril formation by pulmonary surfactant protein C. *FEBS Lett.* **464**, 138–142
- Kallberg, Y., Gustafsson, M., Persson, B., Thyberg, J., and Johansson, J. (2001) Prediction of amyloid fibril-forming proteins. *J. Biol. Chem.* **276**, 12945–12950
- Szyperski, T., Vandenbussche, G., Curstedt, T., Ruysschaert, J. M., Wüthrich, K., and Johansson, J. (1998) Pulmonary surfactant-associated polypeptide C in a mixed organic solvent transforms from a monomeric α -helical state into insoluble β -sheet aggregates. *Protein Sci.* **7**, 2533–2540
- Willander, H., Askarieh, G., Landreh, M., Westermark, P., Nordling, K., Keränen, H., Hermansson, E., Hamvas, A., Noguee, L. M., Bergman, T., Saenz, A., Casals, C., Åqvist, J., Jörnvall, H., Berglund, H., Presto, J.,

- Knight, S. D., and Johansson, J. (2012) High-resolution structure of a BRICHOS domain and its implications for anti-amyloid chaperone activity on lung surfactant protein C. *Proc. Natl. Acad. Sci. U.S.A.* **109**, 2325–2329
17. Mingarro, I., Nilsson, I., Whitley, P., and von Heijne, G. (2000) Different conformations of nascent polypeptides during translocation across the ER membrane. *BMC Cell Biol.* **1**, 3
 18. Johansson, J., Some, M., Linderholm, B. M., Almlén, A., Curstedt, T., and Robertson, B. (2003) A synthetic surfactant based on a poly-Leu SP-C analog and phospholipids: effects on tidal volumes and lung gas volumes in ventilated immature newborn rabbits. *J. Appl. Physiol.* **95**, 2055–2063
 19. Nerelius, C., Martin, E., Peng, S., Gustafsson, M., Nordling, K., Weaver, T., and Johansson, J. (2008) Mutations linked to interstitial lung disease can abrogate anti-amyloid function of prosurfactant protein C. *Biochem. J.* **416**, 201–209
 20. Johansson, H., Nerelius, C., Nordling, K., and Johansson, J. (2009) Preventing amyloid formation by catching unfolded transmembrane segments. *J. Mol. Biol.* **389**, 227–229
 21. Nerelius, C., Gustafsson, M., Nordling, K., Larsson, A., and Johansson, J. (2009) Anti-amyloid activity of the C-terminal domain of pro-SP-C against amyloid β -peptide and medin. *Biochemistry* **48**, 3778–3786
 22. Willander, H., Presto, J., Askarieh, G., Biverstål, H., Frohm, B., Knight, S. D., Johansson, J., and Linse, S. (2012) BRICHOS domains efficiently delay fibrillation of amyloid β -peptide. *J. Biol. Chem.* **287**, 31608–31617
 23. Hermansson, E., Schultz, S., Crowther, D., Linse, S., Winblad, B., Westermarck, G., Johansson, J., and Presto, J. (2014) The chaperone domain BRICHOS prevents CNS toxicity of amyloid- β peptide in *Drosophila melanogaster*. *Dis. Model Mech.* **7**, 659–665
 24. Cohen, S. I., Arosio, P., Presto, J., Kurudenkandy, F. R., Biverstål, H., Dolfe, L., Dunning, C., Yang, X., Frohm, B., Vendruscolo, M., Johansson, J., Dobson, C. M., Fisahn, A., Knowles, T. P., and Linse, S. (2015) A molecular chaperone breaks the catalytic cycle that generates toxic A β oligomers. *Nat. Struct. Mol. Biol.* **22**, 207–213
 25. Stewart, G. A., Ridsdale, R., Martin, E. P., Na, C. L., Xu, Y., Mandapaka, K., and Weaver, T. E. (2012) 4-Phenylbutyric acid treatment rescues trafficking and processing of a mutant surfactant protein-C. *Am. J. Respir. Cell Mol. Biol.* **47**, 324–331
 26. Casals, C., Johansson, H., Saenz, A., Gustafsson, M., Alfonso, C., Nordling, K., and Johansson, J. (2008) C-terminal, endoplasmic reticulum-luminal domain of prosurfactant protein C: structural features and membrane interactions. *FEBS J.* **275**, 536–547
 27. Johansson, H., Nordling, K., Weaver, T. E., and Johansson, J. (2006) The Brichos domain-containing C-terminal part of pro-surfactant protein C binds to an unfolded poly-Val transmembrane segment. *J. Biol. Chem.* **281**, 21032–21039
 28. Kozak, M. (1989) Circumstances and mechanisms of inhibition of translation by secondary structure in eucaryotic mRNAs. *Mol. Cell Biol.* **9**, 5134–5142
 29. Lundin, C., Nordström, R., Wagner, K., Windpassinger, C., Andersson, H., von Heijne, G., and Nilsson, I. (2006) Membrane topology of the human seipin protein. *FEBS Lett.* **580**, 2281–2284
 30. Walter, P., and Blobel, G. (1983) Preparation of microsomal membranes for cotranslational protein translocation. *Methods Enzymol.* **96**, 84–93
 31. Lundin, C., Kim, H., Nilsson, I., White, S. H., and von Heijne, G. (2008) Molecular code for protein insertion in the endoplasmic reticulum membrane is similar for N(in)-C(out) and N(out)-C(in) transmembrane helices. *Proc. Natl. Acad. Sci. U.S.A.* **105**, 15702–15707
 32. Casals, C., Herrera, L., Garcia-Barreno, P., and Municio, A. M. (1990) Association of changes in lysophosphatidylcholine metabolism and in microsomal membrane lipid composition to the pulmonary injury induced by oleic acid. *Biochim. Biophys. Acta* **1023**, 290–297
 33. Sáenz, A., López-Sánchez, A., Mojica-Lázaro, J., Martínez-Caro, L., Nin, N., Bagatolli, L. A., and Casals, C. (2010) Fluidizing effects of C-reactive protein on lung surfactant membranes: protective role of surfactant protein A. *FASEB J.* **24**, 3662–3673
 34. Sáenz, A., Cañadas, O., Bagatolli, L. A., Johnson, M. E., and Casals, C. (2006) Physical properties and surface activity of surfactant-like membranes containing the cationic and hydrophobic peptide KLA. *FEBS J.* **273**, 2515–2527
 35. Perczel, A., Park, K., and Fasman, G. D. (1992) Deconvolution of the circular dichroism spectra of proteins: the circular dichroism spectra of the antiparallel β -sheet in proteins. *Proteins* **13**, 57–69
 36. Cañadas, O., García-Verdugo, I., Keough, K. M., and Casals, C. (2008) SP-A permeabilizes lipopolysaccharide membranes by forming protein aggregates that extract lipids from the membrane. *Biophys. J.* **95**, 3287–3294
 37. Sáenz, A., Cañadas, O., Bagatolli, L. A., Sánchez-Barbero, F., Johnson, M. E., and Casals, C. (2007) Effect of surfactant protein A on the physical properties and surface activity of KLA-surfactant. *Biophys. J.* **92**, 482–492
 38. Whitley, P., Nilsson, I. M., and von Heijne, G. (1996) A nascent secretory protein may traverse the ribosome/endoplasmic reticulum translocase complex as an extended chain. *J. Biol. Chem.* **271**, 6241–6244
 39. Nilsson, I. M., and von Heijne, G. (1993) Determination of the distance between the oligosaccharyltransferase active site and the endoplasmic reticulum membrane. *J. Biol. Chem.* **268**, 5798–5801
 40. Stefansson, A., Armulik, A., Nilsson, I., von Heijne, G., and Johansson, S. (2004) Determination of N- and C-terminal borders of the transmembrane domain of integrin subunits. *J. Biol. Chem.* **279**, 21200–21205
 41. Marsh, D. (1996) Lateral pressure in membranes. *Biochim. Biophys. Acta* **1286**, 183–223
 42. Calvez, P., Bussièrès, S., Eric Demers, and Saless, C. (2009) Parameters modulating the maximum insertion pressure of proteins and peptides in lipid monolayers. *Biochimie* **91**, 718–733
 43. García-Verdugo, I., Cañadas, O., Taneva, S. G., Keough, K. M., and Casals, C. (2007) Surfactant protein A forms extensive lattice-like structures on 1,2-dipalmitoylphosphatidylcholine/rough-lipopolysaccharide-mixed monolayers. *Biophys. J.* **93**, 3529–3540
 44. Biverstål, H., Dolfe, L., Hermansson, E., Leppert, A., Reifenrath, M., Winblad, B., Presto, J., and Johansson, J. (2015) Dissociation of a BRICHOS trimer into monomers leads to increased inhibitory effect on A β 42 fibril formation. *Biochim. Biophys. Acta* **1854**, 835–843
 45. Fitzen, M., Alvelius, G., Nordling, K., Jörnvall, H., Bergman, T., and Johansson, J. (2009) Peptide-binding specificity of the prosurfactant protein C Brichos domain analyzed by electrospray ionization mass spectrometry. *Rapid Commun. Mass Spectrom.* **23**, 3591–3598
 46. Woolhead, C. A., McCormick, P. J., and Johnson, A. E. (2004) Nascent membrane and secretory proteins differ in FRET-detected folding far inside the ribosome and in their exposure to ribosomal proteins. *Cell* **116**, 725–736
 47. Thomas, A. Q., Lane, K., Phillips, J., 3rd, Prince, M., Markin, C., Speer, M., Schwartz, D. A., Gaddipati, R., Marney, A., Johnson, J., Roberts, R., Haines, J., Stahlman, M., and Loyd, J. E. (2002) Heterozygosity for a surfactant protein C gene mutation associated with usual interstitial pneumonitis and cellular nonspecific interstitial pneumonitis in one kindred. *Am. J. Respir. Crit. Care Med.* **165**, 1322–1328
 48. Noguee, L. M., Dunbar, A. E., 3rd, Wert, S. E., Askin, F., Hamvas, A., and Whitsett, J. A. (2001) A mutation in the surfactant protein C gene associated with familial interstitial lung disease. *New Engl. J. Med.* **344**, 573–579
 49. Schamel, W. W., Kuppig, S., Becker, B., Gimborn, K., Hauri, H. P., and Reth, M. (2003) A high-molecular-weight complex of membrane proteins BAP29/BAP31 is involved in the retention of membrane-bound IgD in the endoplasmic reticulum. *Proc. Natl. Acad. Sci. U.S.A.* **100**, 9861–9866
 50. Kota, J., and Ljungdahl, P. O. (2005) Specialized membrane-localized chaperones prevent aggregation of polytopic proteins in the ER. *J. Cell Biol.* **168**, 79–88
 51. Adu-Gyamfi, E., Soni, S. P., Xue, Y., Digman, M. A., Gratton, E., and Stahelin, R. V. (2013) The Ebola virus matrix protein penetrates into the plasma membrane: a key step in viral protein 40 (VP40) oligomerization and viral egress. *J. Biol. Chem.* **288**, 5779–5789
 52. Ji, S. R., Wu, Y., Zhu, L., Potempa, L. A., Sheng, F. L., Lu, W., and Zhao, J. (2007) Cell membranes and liposomes dissociate C-reactive protein (CRP) to form a new, biologically active structural intermediate: mCRP(m). *FASEB J.* **21**, 284–294
 53. Engel, M. F., Yigitpoglu, H., Elgersma, R. C., Rijkers, D. T., Liskamp, R. M., de Kruijff, B., Höppener, J. W., and Antoinette Killian, J. (2006) Islet amyloid polypeptide inserts into phospholipid monolayers as monomer. *J. Mol.*

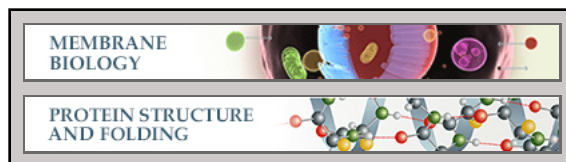
- Biol.* **356**, 783–789
54. Beers, M. F., and Mulugeta, S. (2005) Surfactant protein C biosynthesis and its emerging role in conformational lung disease. *Annu. Rev. Physiol.* **67**, 663–696
55. Bridges, J. P., Wert, S. E., Noguee, L. M., and Weaver, T. E. (2003) Expression of a human surfactant protein C mutation associated with interstitial lung disease disrupts lung development in transgenic mice. *J. Biol. Chem.* **278**, 52739–52746
56. Woischnik, M., Sparr, C., Kern, S., Thurm, T., Hector, A., Hartl, D., Liebisch, G., Mulugeta, S., Beers, M. F., Schmitz, G., and Griese, M. (2010) A non-BRICHOS surfactant protein c mutation disrupts epithelial cell function and intercellular signaling. *BMC Cell Biol.* **11**, 88
57. Beers, M. F., Hawkins, A., Maguire, J. A., Kotorashvili, A., Zhao, M., Newitt, J. L., Ding, W., Russo, S., Guttentag, S., Gonzales, L., and Mulugeta, S. (2011) A nonaggregating surfactant protein C mutant is misdirected to early endosomes and disrupts phospholipid recycling. *Traffic* **12**, 1196–1210
58. Thiele, J. R., Habersberger, J., Braig, D., Schmidt, Y., Goerendt, K., Maurer, V., Bannasch, H., Scheichl, A., Woollard, K. J., von Dobschütz, E., Kolodgie, F., Virmani, R., Stark, G. B., Peter, K., and Eisenhardt, S. U. (2014) Dissociation of pentameric to monomeric C-reactive protein localizes and aggravates inflammation: *in vivo* proof of a powerful proinflammatory mechanism and a new anti-inflammatory strategy. *Circulation* **130**, 35–50
59. Zavialov, A. V., and Knight, S. D. (2007) A novel self-capping mechanism controls aggregation of periplasmic chaperone Caf1M. *Mol. Microbiol.* **64**, 153–164
60. Haslbeck, M., Franzmann, T., Weinfurter, D., and Buchner, J. (2005) Some like it hot: the structure and function of small heat-shock proteins. *Nat. Struct. Mol. Biol.* **12**, 842–846
61. Cañadas, O., and Casals, C. (2013) Differential scanning calorimetry of protein-lipid interactions. *Methods Mol. Biol.* **974**, 55–71

Membrane Biology:
Folding and Intramembraneous BRICHOS
Binding of the Prosurfactant Protein C
Transmembrane Segment

Alejandra Sáenz, Jenny Presto, Patricia Lara,
Laura Akinyi-Oloo, Belén García-Fojeda,
IngMarie Nilsson, Jan Johansson and Cristina
Casals

J. Biol. Chem. 2015, 290:17628-17641.

doi: 10.1074/jbc.M114.630343 originally published online June 3, 2015



Access the most updated version of this article at doi: [10.1074/jbc.M114.630343](https://doi.org/10.1074/jbc.M114.630343)

Find articles, minireviews, Reflections and Classics on similar topics on the [JBC Affinity Sites](https://www.jbc.org/).

Alerts:

- [When this article is cited](#)
- [When a correction for this article is posted](#)

[Click here](#) to choose from all of JBC's e-mail alerts

This article cites 61 references, 21 of which can be accessed free at
<http://www.jbc.org/content/290/28/17628.full.html#ref-list-1>